# BMEye: Public Health-Oriented Body Mass Index Monitoring using Commodity WiFi

Kiran Davuluri*, Khairul Mottakin*, Zheng Song*, Jin Lu†, Mark Allison‡
*Dept. of Computer and Information Science, University of Michigan-Dearborn, MI, USA
{*kirandav, khairulm, zhesong*}*@umich.edu*
† School of Computing, University of Georgia, GA, USA, *jin.lu@uga.edu*
‡ College of Innovation and Technology, University of Michigan-Flint, MI, USA, *markalli@umich.edu*

***Abstract*—Body Mass Index (BMI) is a commonly used measure of body fat based on an individual's height and weight. Public health authorities and organizations monitor BMI at a population level to assess the prevalence and trends of underweight and obesity within communities. This helps identify at-risk populations, evaluate the effectiveness of interventions, and develop targeted strategies to promote healthy weight and prevent associated health problems. However, there is a lack of BMI monitoring methods that do not require active cooperation or cause privacy concerns to human subjects. This paper introduces a BMI classification approach based on passive WiFi sensing. Our proposed approach is inspired by the observation that different body shapes cause dissimilar impacts on WiFi signal propagation, which can be reflected by Channel State Information (CSI) readings. Leveraging state-of-the-art machine learning algorithms, we developed a BMI sensing system that classifies the BMI of human subjects when they move in a WiFi range. Our evaluation results show that our approach could be an effective tool for public-health-oriented BMI monitoring, yielding a precision rate of 70.86%, a recall rate of 71.21%, and an F1 score of 73.66%.**

***Index Terms*—Channel State Information (CSI), WiFi Sensing, Machine Learning, BMI Classification, Public Health**

## I. Introduction

The Body Mass Index (BMI), calculated based on an individual's weight and height, has been found to significantly correlate with body fat levels [1]. In light of the widespread obesity epidemic, community-based monitoring of BMI has emerged as an effective public health tool that is employed extensively on a global scale [2]. It helps identify at-risk populations and neighborhoods, evaluate the effectiveness of interventions, and develop targeted strategies to promote healthy weight and prevent associated health problems.

Existing methods for BMI monitoring can be categorized into three main approaches: 1) obtaining patients' records from health care systems [3], which incurs no additional cost but may fail to provide fine-grained data while raising privacy concerns; 2) recruiting participants and relying on self-reported height and weight information is a resource-intensive approach [4], making it impractical for long-term monitoring; 3) capturing images of individuals and utilizing image processing and machine learning techniques to estimate BMI has shown promise [5], [6], but it also raises privacy concerns. Considering the significant impact of BMI monitoring on public health, there is a pressing need for a monitoring approach that is fine-grained, cost-effective and respects privacy. Such an approach would allow for detailed data collection at a more localized level, be feasible for long-term implementation, and not compromise the privacy of individuals.

To solve this problem, we introduce a novel WiFi-sensing-based BMI classification approach, which is inspired by the observation that a moving person of different shapes may cause different impacts on the reflection and refraction of a WiFi signal. Our approach requires a human subject to pass a sensing region formed by commodity WiFi devices, collects time series of WiFi Channel State Information (CSI) signals to capture the impacts, and applies machine learning techniques for BMI classification.

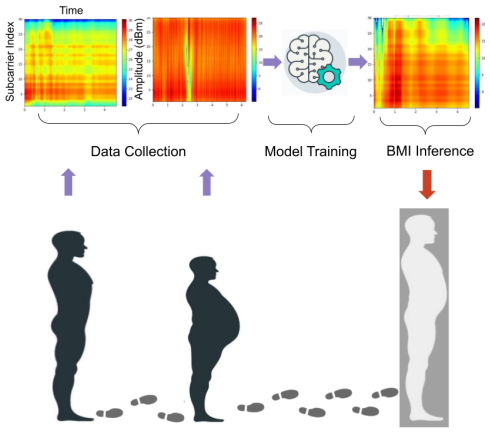


Fig. 1: Illustration of CSI-based BMI classification

Fig. 1 demonstrates the workflow of our approach. When a human subject moves in a region covered by WiFi, WiFi signals sent from the transmitter to the receiver are distorted by the human. Such minor disruptions can be captured by the time series of CSI and analyzed by machine learning algorithms to determine the characteristics of the objects causing disruptions [7]. By collecting CSI from human subjects with varied BMI walking across a certain region, a classification model is trained for estimating the BMI of an unknown subject based on his CSI data.

The key contributions of our work are summarized below:

- We introduce a novel BMI monitoring approach based on WiFi sensing. With the rapid advancements in collecting and processing CSI, WiFi sensing is being integrated into

emerging WiFi standards like WiFi 7 [8]. Our approach offers a fine-grained, affordable, and privacy-friendly solution for monitoring BMI, which holds significant potential for enhancing public health when WiFi 7 becomes more widely adopted.
- We set up a WiFi sensing system using off-the-shelf devices to collect CSI. Using our system, we collected CSI data for 30 human subjects with varied BMI. We release our collected data for public access [1].
- We employ state-of-the-art machine learning algorithms to train BMI classification models and report their evaluation results. Our ResNet-based model achieved a precision rate of 70.86%, a recall rate of 71.21%, and an F1 score of 73.66%.

The remainder of this paper is organized as follows: Section II provides a review of work in the related domain. Section III introduces our methodology, and Section IV reports how we evaluated the effectiveness of our approach. Section V discusses the inferences that can be deduced from the results. Finally, we conclude this paper with Section VI.

## II. Related Works

### A. Channel State Information (CSI)

Fine-grained CSI is frequently used to characterize the propagation of a WiFi signal as it comes in contact with obstacles [9]. All WiFi standards use OFDM modulation, which distributes available bandwidth across multiple sub-carriers [10]. While RSSI (Received Signal Strength Indicator) averages the signal strength across all sub-carriers and provides one reading for a received WiFi signal, CSI catches changes occurring at each sub-carrier and provides more fine-grained measurements. CSI is characteristically described as a 3-way channel tensor for *t* transmitting and *r* receiving antennas:

$$CSI = \begin{bmatrix} H_{1,1} & \dots & H_{1,r} \\ \vdots & \ddots & \vdots \\ H_{t,1} & \dots & H_{t,r} \end{bmatrix} \quad (1)$$

, where $H_{t,r}$ is a vector that includes complex pairs for each sub-carrier, as given in Eq. (2).

$$H_{t,r} = [h_{t,r,1}, \dots, h_{t,r,m}] \quad (2)$$

The number of sub-carriers differs based on the hardware and the channel bandwidth. For *m* data sub-carrier, $H_{t,r}$ is expressed as complex number $h_m$, containing both amplitude($|h_m|$) and phase($\angle h_m$) of the CSI. Due to multi-path effects such as phase shift and amplitude attenuation, the CSI amplitude and phase values are affected by human movements [11], which is often used to accurately sense the behavior and location of the human subject.

[1]https://github.com/kiran-collab/CSIKit-BMI

### B. BMI Classification

BMI estimates the body fat of a person by his mass and height: BMI = Weight(lb) / [Height(in)]$^2$ $\times$ 703. It helps ascertain risk factors for health conditions. Adults can be classified into four categories, namely "*Obese*", "*Overweight*", "*Normal Weight*", and "*Underweight*" based on their BMIs. Fig. 2 shows how weight and height impact BMI classification.

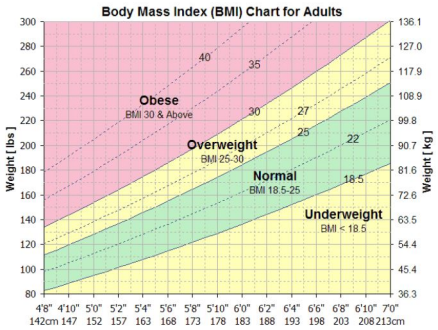

Fig. 2: BMI Chart for Adults

Sec. I presents an array of methods for BMI monitoring. Recent attention has gravitated towards computer-vision-based BMI assessment, a method that avoids the need for participant recruitment or retrieval of patient records. This method's potential for seamless integration into everyday living and working environments is notable. However, it triggers privacy concerns [12].

### C. WiFi Sensing

Bio-electromagnetic studies for WiFi [13], specifically for 2.4G WiFi and 5G WiFi show that feature traits/gestures are efficiently captured when an electromagnetic radiation wave propagates at specific frequencies(e.g., 2.45GHz). The observation builds the foundation for WiFi sensing. In the last decade, there have been many applications [14] that leverage wireless channels to build applications in human-computer interaction [15], healthcare [16], and surveillance [17].

Inspired by the concept of unique pattern generation for active motion in the sensing region [18], body characterization research focuses on pose, person, gait, and activity recognition using statistical features extracted from CSI sequences [19]–[21]. Deep learning (DL) methods have been explored to enhance feature extraction from CSI data, thereby enhancing the robustness of CSI-based body characterization [10], [22]. Challenges such as overfitting and limited datasets persist, requiring dedicated layers for specific datasets. DL has shown success in sensorless body characterization and human activity recognition by applying transformation methods, with applications ranging from activity detection frameworks to small-scale recognition systems that address signal variations caused by movement speeds and body shapes [23].

## III. Methodology

### A. Overview

Figure 3 presents an overview of our system, illustrating the process of collecting and processing Channel State Informa-

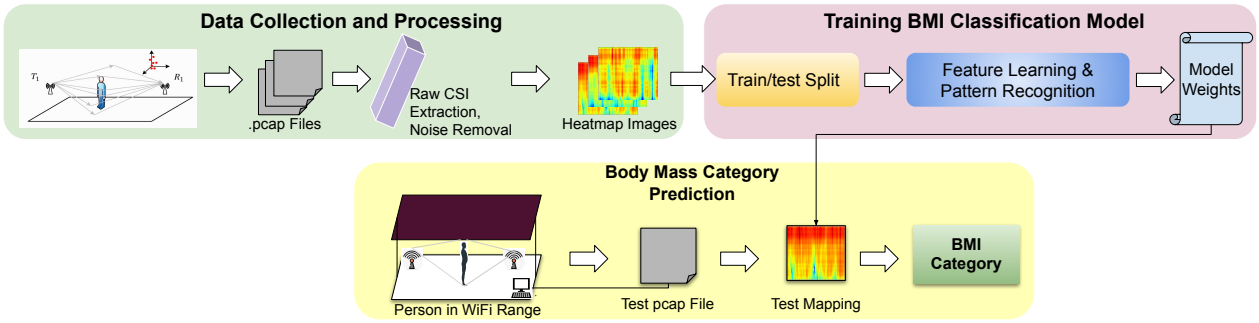


Fig. 3: General Workflow of BMEye

tion (CSI) data for BMI prediction in practical scenarios. In order to design a system that is applicable and deployable in real-world settings, we collected extensive data from subjects participating in various trials. This dataset encompasses a diverse range of body shapes, walking speeds, and movements, including rotation, walking backward, sideways, and more. This approach ensures the system's effectiveness and robustness in categorizing body mass in real-world scenarios. To facilitate BMI classification, we generated heatmaps in the form of 2D images. The numerical CSI is represented on a two-dimensional grid using color gradients, where the color intensity corresponds to the data value. These heatmaps serve as input for training traditional as well as advanced machine learning architectures.

### B. Hardware Selection

For our experimental setup, we utilized Raspberry Pi (RPi), a readily available commodity device. An alternative choice is the Intel 5300 Network Interface Card (NIC) [24], which has become less prevalent due to its limited availability in the current market. On the contrary, RPis has emerged as a more suitable option for WiFi-based healthcare monitoring in commercial and smart home environments due to its affordability and potential capabilities. To enable the necessary monitoring capabilities, we utilized the Nexmon tool, which supports the monitoring of specific frames, up to 80 MHz bandwidth, and 256 sub-carriers [25].

### C. Data Collection

| BMI Category | Class Distribution (out of 1) | Age Distribution (in yrs) | Gender Ratio (Male:Female) | Weight Range (in kg) | Height Range (in m) |
|---|---|---|---|---|---|
| ***Underweight*** | 0.133 | 19-25 | 4:0 | 50.4-57.0 | 1.67-1.78 |
| ***Normal*** | 0.6 | 23-40 | 13:5 | 53.8-75.5 | 1.63-1.86 |
| ***Overweight*** | 0.133 | 19-40 | 3:1 | 69.3-87.4 | 1.57-1.69 |
| ***Obese*** | 0.133 | 30-50 | 4:0 | 87.7-119.9 | 1.62-1.81 |

TABLE I: Participants Distribution

We randomly recruited 30 participants from the CIS department at UMDearborn. Their body weights and heights were measured and utilized to calculate their respective BMIs. We also documented each participant's gender and age. Additional details about our participants can be found in Table I.

We asked the participants to walk in an indoor lab room *(6m x 6m)* on specified trails and recorded the CSI samples when they walked, as depicted in Fig. 4. The first two trails involved walking (0.3 - 0.8 m/s) from the start to the end of the defined paths. The paths were of length *3m* each, for which

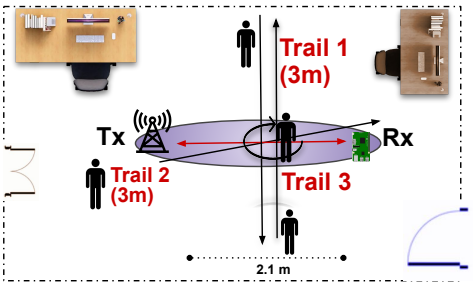


Fig. 4: CSI Collection System Setup

*25* and *10* samples were collected respectively. The third trial involves rotating(turning 90 degrees every 2 secs) at the center of the Line of Sight(LoS), 5 times each.

| System Settings | |
|---|---|
| ***Tx-Rx Height*** | 0.5m |
| ***Tx-Rx Distance*** | 2.1m |
| ***# of subjects*** | 30 |
| ***Subject Movements/ Activity*** | Walking, Rotation |
| ***# of trails*** | 3 |
| ***Sampling duration*** | 4-8 sec |
| ***Sampling rate*** | 200 Hz |
| ***CSI samples*** | 1050 |
| ***Channel Frequency*** | 80 MHz |

TABLE II: System Settings

The layout of the ensemble lies approximately in the center of the room. An RPi, acting as a passive observer (Rx), measured the CSI of WiFi signals sent by an Access Point (Tx) positioned approximately *2m* away. A computer connected to the router generates traffic by sending 8000 ping packets to the Tx, and the RPi worked in monitor mode to capture data for each pong packet. We experimentally choose the number of packets generated according to the movement duration. The CSI sampling rate was set to 200 Hz, which is fast enough to capture the movement of subjects. CSI data was captured using Nexmon and rendered with *tcpdump*, which produces a .pcap file. This file is then interpreted using CSIKit which generates 256 x 1 numpy matrices, which can then be used in *Tensorflow*. From these, the CSI amplitude is derived. The raw amplitude values are then windowed using a sliding window of 1 second at 100Hz, with an overlap of 1 second. Table II summarizes the settings of our data collection system.

### D. Data Processing

The heatmaps in Fig.1 (in Sec. I) were generated using CSIKit [26]. They are pseudo colormaps that interpret signal variation across time, sub-carriers, and amplitude into 3-channel(RGB) color intensities. The x-axis represents the timeline, the y-axis represents sub-carriers, and the z-axis (color intensity) represents CSI amplitude. To mitigate noise in the collected CSI data from the Raspberry Pi while preserving the waveform, a Least-square smoothing filter [27] was applied using a sample window of size 51.

OFDM technology utilizes null, pilot, and data sub-carriers [28]. Null sub-carriers protect against interference, pilot sub-carriers aid in synchronization, and data sub-carriers carry modulated data. After removing null and pilot sub-carriers, complex numbers representing CSI phase and amplitude are extracted. Each sub-carrier is crucial for accurate recognition due to variations caused by human reflections. Having a higher proportion of sub-carriers provides more information and improves feature detection for analysis.

### E. Training for BMI Classification

We collected a total of 1050 sampled 2D CSI images, and we randomly choose 900 samples for training and the remaining 150 for testing, as depicted in Table III. In the training set, we chose 20% samples as the validation set.

Table I reveals an imbalanced distribution of collected samples across different classes. To address this bias, class weights were calculated by dividing the number of samples per class by the total number of samples and taking the reciprocal. The resulting class weights for the four classes are: *0.0082*, *0.0018*, *0.0079*, and *0.0090*. Notably, the *Normal Weight* class contains significantly more samples, causing the bias, which is mitigated during training using a weighted random sampler and the calculated class weights. Gender bias was not considered due to the gender-neutral BMI ranges [29]. Fig. 5 illustrates the feature extraction process in the training pipeline of the learning architectures which was implemented using *PyTorch*.

**ResNet-50 & EffNet.** The training and test datasets were preprocessed with random resizing, cropping, horizontal flipping, and normalization. The models were initialized with pre-trained weights from ImageNet and had their last fully connected layer replaced with a linear layer for the specific classification task. During training, *ResNet* is optimized using stochastic gradient descent (SGD) while the *EffNet* was optimized with Adam optimizer. Both the backbones were tuned with a learning rate of 0.001 and momentum of 0.9. The models were trained for 15 epochs. Both models were trained for 15 epochs with a mini-batch size of 32, updating parameters based on the cross-entropy loss function. Validation accuracy was calculated after each epoch to monitor performance on unseen data.

## IV. Evaluation

This section reports the evaluation results of the trained networks, as well as the insight we gained into CSI-based BMI classficiation through visualization and data variation analysis.

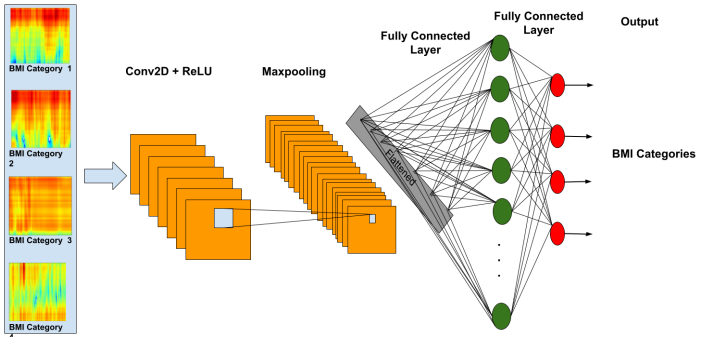


Fig. 5: Training Neural Networks with Heatmaps as Input

### A. BMI Classification Accuracy

| Architecture /Data Split | Train (0.9k images) | | Test (0.15k images) | | |
|---|---|---|---|---|---|
| | Accuracy (Train & Validation) | | F1 | Precision | Recall |
| ***ResNet-50*** | 0.6844 | 0.6625 | 0.7366 | 0.7086 | 0.7121 |
| ***EffNet-B0*** | 0.4484 | 0.4199 | 0.3999 | 0.6040 | 0.4305 |

TABLE III: Model Performances

Referring to Table III, we see *ResNet-50* performs better than *EffNet-B0* in terms of test precision. For each model, Fig. 6 compares the predicted class labels against the actual class labels overall data instances. For *ResNet-50*, we observe that 1) It obtains the highest True Positives (TP) for the *Normal Weight* category, resulting in a high F1 score (0.7366); 2) It scores similarly on Precision and Recall for the other categories, demonstrating balanced performance. *EffNet-B0*, on the other hand, seems to have difficulties with the *Normal Weight* category, leading to a low F1 score and recall. However, *EffNet* generally exhibits computational efficiency and faster inference time. Assuming its accuracy can be improved, *EffNet* could be well-suited for deployment on resource-limited IoT devices like RPis.

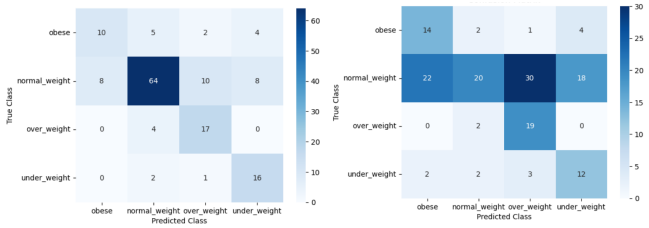


(a) ResNet-50 (b) EffNet-B0

Fig. 6: Confusion Matrices

### B. Data Visualization and Variation Analysis

In this subsection, we perform two crucial analyses, namely t-SNE visualization and data variation analysis, to gain deeper insights into the CSI heatmap data. The t-SNE visualization allows us to visually explore the high-dimensional CSI data by reducing its dimensions into a 2D or 3D representation. This visual exploration aids in uncovering potential patterns, relationships, or anomalies that may not be immediately apparent

in the original dataset. On the other hand, the data variation analysis focuses on quantifying the extent of variability and changes within the CSI data.

1) **T-SNE.** To visualize the high-dimensional data in a consistent manner, we used t-SNE ((t-Distributed Stochastic Neighbor Embedding)) [30], which was used in *Python*. t-SNE transforms similarities among data points into joint probabilities, minimizing the Kullback-Leibler divergence. The resulting scatterplot (Fig. 7) was created using *matplotlib library*, where each point represents a data point's primary features. The t-SNE dimensions are nonlinear combinations of the original dimensions, and reflect the projection of the data into a lower-dimensional space, preserving relationships between data points in the two spaces.

Utilizing virtualization techniques, our analysis uncovers distinctive clustering patterns within the CSI data. Each distinct color in the visual representation corresponds to a specific BMI class. Remarkably, our observations indicate a notable inclination for obese samples to form clusters in close proximity to overweight samples, as evidenced by the isolated upper cluster. Conversely, underweight samples exhibit a propensity to cluster alongside normal weight samples, as illustrated in the rightmost bottom and central regions of the figure. This visualization corroborates the classification performance depicted in Figure 6, wherein the model exhibited a consistent pattern of misclassifying samples. As a result, these findings suggest the potential for future enhancements in the model, contingent upon addressing the presence of noise within the collected CSI data.

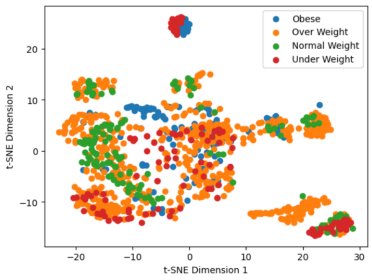


Fig. 7: Data visualization using t-SNE

**2) Variation Analysis.** Further, we find semantic variations in the mappings of distinct classes. We evaluate ***Average Distance(AD)***, ***Degree of Intersection(DoI)*** for the (*Underweight & Normal Weight*) and (*Underweight & Obese*) label sets. For each method, we calculate the metric value for three different image pairs and compute its mean ***(mAD, mDoI)***. This process is repeated for three sets of class pairs (ref. IV), ensuring generalization across the entire data range. The following techniques were employed to compute the features and calculate the aforementioned metrics:

**Scale Invariant Feature Transform.** SIFT extracts key features and descriptors from the images. The descriptors of one image are matched from each descriptor of the other in terms of distance. The match values are then sorted by distance. The Average Distance is calculated by the total distance over all the matches.

| Metric/Classes/Setup | **Mean Avg. Distance (SIFT)** | **Mean Degree of Intersection (Histogram Analysis)** |
|---|---|---|
| ***Under Weight & Normal Weight (Set 1)*** | 137.59 | 0.8055 |
| ***Under Weight & Obese (Set 2)*** | 165.57 | 0.6899 |
| ***Normal Weight & Obese (Set 3)*** | 139.59 | 0.7134 |

TABLE IV: Data Variations for Different Classes

**Histogram Comparison.** Histogram comparison measures the intersection between normalized histograms to analyze pattern dissimilarity. The method calculates the sum of the minimum values for each bin in the two histograms. This sum represents the intersection between the histograms.

Although the computed measures depend on various factors, such as the presence of noise, and distortions, we can infer from Table IV, that *mAD* for all the sets of label pairs is high. For similar images, the values must be relatively low. Also, there is a considerable difference in the values for the corresponding class pairs. We see similar traits for the other metric. In the case of the first set, *mDoI* is high as the classes are immediate, whereas *mDoI* for Set 2 is contrastively lesser, showing the variation of data from the three classes.

Overall, the t-SNE visualization analysis and the data variation analysis provide complementary perspectives on understanding the underlying patterns and relationships within the dataset. We adopted t-SNE to visually explore and identify clusters. On the other hand, our data variation analysis focuses on quantifying the extent of variability and changes within the CSI data across different classes. By analyzing the designed metrics, our data variation analysis presents the degree of separability between the classes in the CSI data. Together, these analyses contribute to a comprehensive understanding of our collected CSI dataset, combining visual exploration and quantitative assessment to gain insights into the data.

## V. Discussion and Future Work

When conducting the experiments, we observed a few factors that could potentially alter the heatmap, thereby influencing the accuracy of BMI classification:

- Environmental factors, such as room layout and the number of people in the room, airflow of air conditioner, and interfering signals from electronic devices.
- Human body factors, such as hand positions and clothing.
- Movement factors, such as speed and patterns of movement. In particular, we observed that data for a person near the transmitter exhibited greater robustness compared to that at the receiver end. We also noticed that for a person with very slow movement, the body characteristics can be easily deciphered vide sub-carrier variation where there is a sudden shift in pixel intensities. For regular or speed movement, time-wise variation with displacement(via spatial inference) can be employed.
- Location of WiFi devices. For instance, when the receiver and transmitter were placed on opposite sides of the subject, but at different height levels (one at head level and one at foot level), the heatmap readings significantly

varied from our setup. An additional future direction involves experimenting with different configurations to identify the most optimal setting for the proposed system.

For our experiment, we controlled all variables such as the subjects' movement speeds, clothing styles, walking patterns (e.g., no hand waving), and their paths. However, due to the impact of these factors and the limited dataset we collected, the performance of our models can still be improved. Moving forward, we plan to compile a more extensive dataset and design custom neural networks for body mass estimation.

## VI. Conclusion

This paper presents a simple yet efficient approach that measures BMI for public health monitoring. We collected CSI data from 30 participants using off-the-shelf WiFi devices and converted the data to image mappings. These images were fed with machine learning backbones for BMI classification. Our evaluation results demonstrate the effectiveness of our approach in practical settings.

To the best of our knowledge, this study pioneers the use of WiFi sensing for public health-oriented BMI monitoring. In our forthcoming research, we intend to delve deeper into the stability of this technique when individuals exhibit more unrestricted movements. Additionally, we aim to collect a larger-scale, more comprehensive dataset to further improve the accuracy of our ML models.

## Acknowledgment

This research is supported by NSF through grants 2104337 and 2122309. We also thank Jerome Marudo for his contribution to this work, and the volunteers who participated in our data collection.

## References

[1] S. B. Wyatt, K. P. Winters, and P. M. Dubbert, "Overweight and obesity: prevalence, consequences, and causes of a growing public health problem," *The American journal of the medical sciences*, vol. 331, no. 4, pp. 166–174, 2006.

[2] G. Nasser, "Fighting childhood obesity in brazil: a grassroots perspective," *European Journal of Public Health*, vol. 30, no. Supplement_5, pp. ckaa166–474, 2020.

[3] P. Anthamatten, D. S. Thomas, D. Williford, J. C. Barrow, K. A. Bol, A. J. Davidson, S. J. Deakyne Davies, E. M. Kraus, D. C. Tabano, and M. F. Daley, "Geospatial monitoring of body mass index: use of electronic health record data across health care systems," *Public Health Reports*, vol. 135, no. 2, pp. 211–219, 2020.

[4] J. S. Fish, S. Ettner, A. Ang, and A. F. Brown, "Association of perceived neighborhood safety on body mass index," *American journal of public health*, vol. 100, no. 11, pp. 2296–2303, 2010.

[5] Z. Jin, J. Huang, W. Wang, A. Xiong, and X. Tan, "Estimating human weight from a single image," *IEEE Transactions on Multimedia*, 2022.

[6] J. C. Gonzales, J. R. G. Garcia, and J. F. Villaverde, "Bmi estimation from 2d face images using support vector machine," in *2022 6th International Conference on Communication and Information Systems (ICCIS)*. IEEE, 2022, pp. 118–123.

[7] Y. Ge, J. Wang, S. Li, L. Qi, S. Zhu, J. Cooper, M. Imran, and Q. H. Abbasi, "Wifi sensing of human activity recognition using continuous aoa-tof maps," in *2023 IEEE Wireless Communications and Networking Conference (WCNC)*, 2023, pp. 1–6.

[8] V. Frascolla, D. Cavalcanti, and R. Shah, "Wi-fi evolution: The path towards wi-fi 7 and its impact on iiot," *Journal of Mobile Multimedia*, vol. 19, no. 01, p. 263–276, Sep. 2022. [Online]. Available: https://journals.riverpublishers.com/index.php/JMM/article/view/18515

[9] N. Zhou, W. Sun, and M. Liang, "Human activity recognition based on wifi signal using deep neural network," in *International Conference on Smart City and Informatization (iSCI)*. IEEE, 2020, pp. 26–30.

[10] S. Yousefi, H. Narui, S. Dayal, S. Ermon, and S. Valaee, "A survey on behavior recognition using wifi channel state information," *IEEE Communications Magazine*, vol. 55, no. 10, pp. 98–104, 2017.

[11] T. Xin, B. Guo, Z. Wang, P. Wang, J. C. K. Lam, V. Li, and Z. Yu, "Freesense: A robust approach for indoor human detection using wi-fi signals," *Proceedings of the ACM on Interactive, Mobile, Wearable and Ubiquitous Technologies*, vol. 2, no. 3, pp. 1–23, 2018.

[12] J. S. Kumar and D. R. Patel, "A survey on internet of things: Security and privacy issues," *International Journal of Computer Applications*, vol. 90, no. 11, 2014.

[13] S. Gabriel, R. Lau, and C. Gabriel, "The dielectric properties of biological tissues: Ii. measurements in the frequency range 10 hz to 20 ghz," *Physics in medicine & biology*, vol. 41, no. 11, p. 2251, 1996.

[14] Y. Ma, G. Zhou, and S. Wang, "Wifi sensing with channel state information: A survey," *ACM Computing Surveys (CSUR)*, vol. 52, no. 3, pp. 1–36, 2019.

[15] K. Qian, C. Wu, Z. Zhou, Y. Zheng, Z. Yang, and Y. Liu, "Inferring motion direction using commodity wi-fi for interactive exergames," in *Proceedings of the 2017 CHI conference on human factors in computing systems*, 2017, pp. 1961–1972.

[16] X. Wang, C. Yang, and S. Mao, "Tensorbeat: Tensor decomposition for monitoring multiperson breathing beats with commodity wifi," *ACM Transactions on Intelligent Systems and Technology (TIST)*, vol. 9, no. 1, pp. 1–27, 2017.

[17] X. Zheng, J. Wang, L. Shangguan, Z. Zhou, and Y. Liu, "Smokey: Ubiquitous smoking detection with commercial wifi infrastructures," in *IEEE INFOCOM 2016-The 35th Annual IEEE International Conference on Computer Communications*. IEEE, 2016, pp. 1–9.

[18] P. F. Moshiri, H. Navidan, R. Shahbazian, S. A. Ghorashi, and D. Windridge, "Using gan to enhance the accuracy of indoor human activity recognition," *arXiv preprint arXiv:2004.11228*, 2020.

[19] T. Mabuchi, Y. Taniguchi, and K. Shirahama, "Person recognition using wi-fi channel state information in an indoor environment," in *2020 IEEE International Conference on Consumer Electronics-Taiwan (ICCE-Taiwan)*. IEEE, 2020, pp. 1–2.

[20] F. Wang, S. Zhou, S. Panev, J. Han, and D. Huang, "Person-in-wifi: Fine-grained person perception using wifi," in *Proceedings of the IEEE/CVF International Conference on Computer Vision*, 2019, pp. 5452–5461.

[21] J. Ding, Y. Wang, and X. Fu, "Wihi: Wifi based human identity identification using deep learning," *IEEE Access*, vol. 8, 2020.

[22] J. Zhang, F. Wu, B. Wei, Q. Zhang, H. Huang, S. W. Shah, and J. Cheng, "Data augmentation and dense-lstm for human activity recognition using wifi signal," *IoTJ*, vol. 8, no. 6, pp. 4628–4641, 2020.

[23] W. Qi, R. Zhang, J. Zhou, H. Zhang, Y. Xie, and X. Jing, "A resource-efficient cross-domain sensing method for device-free gesture recognition with federated transfer learning," *IEEE Transactions on Green Communications and Networking*, vol. 7, no. 1, pp. 393–400, 2023.

[24] D. Halperin, W. Hu, A. Sheth, and D. Wetherall, "Tool release: Gathering 802.11 n traces with channel state information," *ACM SIGCOMM computer communication review*, vol. 41, no. 1, pp. 53–53, 2011.

[25] F. Gringoli, M. Schulz, J. Link, and M. Hollick, "Free your csi: A channel state information extraction platform for modern wi-fi chipsets," in *Proceedings of the 13th International Workshop on Wireless Network Testbeds, Experimental Evaluation & Characterization*, 2019, pp. 21–28.

[26] G. Forbes. (2021) Csikit: Python csi processing and visualisation tools for commercial off-the-shelf hardware. [Online]. Available: https://github.com/Gi-z/CSIKit

[27] R. W. Schafer, "What is a savitzky-golay filter? [lecture notes]," *IEEE Signal Processing Magazine*, vol. 28, no. 4, pp. 111–117, 2011.

[28] M. S. Gast, *802.11 ac: a survival guide: Wi-Fi at gigabit and beyond*. " O'Reilly Media, Inc.", 2013.

[29] M. F. Daley, J. C. Barrow, D. C. Tabano, L. M. Reifler, E. M. Kraus, S. D. Davies, D. L. Williford, B. White, A. Shupe, and A. J. Davidson, "Estimating childhood obesity prevalence in communities through multi-institutional data sharing," *Journal of Public Health Management and Practice*, vol. 26, no. 4, pp. E1–E10, 2020.

[30] F. Pedregosa, G. Varoquaux, A. Gramfort, V. Michel, B. Thirion, O. Grisel, M. Blondel, P. Prettenhofer, R. Weiss, V. Dubourg, J. Vanderplas, A. Passos, D. Cournapeau, M. Brucher, M. Perrot, and E. Duchesnay, "Scikit-learn: Machine learning in Python," *Journal of Machine Learning Research*, vol. 12, pp. 2825–2830, 2011.